Regenerative Medicine and Dentistry
https://www.sciltp.com/journals/rmd

Article

Controlled Codelivery of Hydrogen Sulfide and Nitric Oxide for the Treatment of Full-Thickness Skin Wound

Meng Qian [1,2,†], Guangbo Ji [2,†], Pei Liu [2], Yating Zhang [2], Weiliang Deng [2], Zhixin Xu [2], Huan Wang [1], Jiansong Cheng [3] and Qiang Zhao [1,2,*]

[1] The Institute of Cardiovascular Sciences, School of Basic Medical Sciences, State Key Laboratory of Vascular Homeostasis and Remodeling, Health Science Center, Peking University, Beijing 100191, China
[2] State Key Laboratory of Medicinal Chemical Biology, Key Laboratory of Bioactive Materials (Ministry of Education), Frontiers Science Center for Cell Responses, College of Life Sciences, Nankai University, Tianjin 300071, China
[3] College of Pharmacy, Nankai University, Tianjin 300353, China
* Correspondence: qiangzhao@nankai.edu.cn
† These authors contributed equally to this work.

How To Cite: Qian, M.; Ji, G.; Liu, P.; et al. Controlled Codelivery of Hydrogen Sulfide and Nitric Oxide for the Treatment of Full-Thickness Skin Wound. *Regenerative Medicine and Dentistry* **2025**, *2*(3), 13. https://doi.org/10.53941/rmd.2025.100013

Received: 28 July 2025
Revised: 15 August 2025
Accepted: 17 September 2025
Published: 19 September 2025

Abstract: Chronic wounds present significant clinical challenges stemming from persistent inflammation, impaired angiogenesis, and disrupted tissue homeostasis. Nitric oxide (NO) and hydrogen sulfide (H_2S) are important gaseous signalling molecules that play critical regulatory roles in the pathophysiology of numerous diseases. In the present study, we designed a novel prodrug, TSNO, which releases H_2S and NO in a controlled manner under the catalysis of GSH and the engineered enzyme A4-β-Gal^{H363A}. Furthermore, a functional wound dressing was prepared by incorporating TSNO into an electrospun poly(ε-caprolactone) (PCL) mat, and the therapeutic efficacy was evaluated in a full-thickness skin wound model established in mice. Results showed that the functional wound dressing effectively accelerated the wound healing process by enhancing collagen synthesis, promoting angiogenesis, and regulating inflammation via controlled codelivery of H_2S and NO. Taken together, the functional wound dressing developed in this study represents a promising candidate for treating large-scale skin wounds in the clinic.

Keywords: hydrogen sulfide; nitric oxide; codelivery; enzyme-prodrug technology (EPT); wound healing

1. Introduction

The skin serves as an effective barrier for the human body, preventing pathogen invasion and protecting internal organs. Wound healing is a continuous and overlapping process that includes inflammation, proliferation, and tissue remodeling [1]. Each phase requires specific interventions, such as inflammation control, promotion of angiogenesis, and modulation of homeostasis, which involve many different cell types, growth factors, cytokines, and other agents [2,3]. Up to now, impaired cutaneous wound repair remains a great clinical challenge, which warrants the development of novel strategies to accelerate wound healing.

Nitric oxide (NO) and hydrogen sulfide (H_2S) are important signalling molecules that play vital roles in multiple physiological processes [4–6]. Endogenous NO is produced primarily from the substrate L-arginine by three different isoforms of nitric oxide synthase (NOS). Both eNOS and iNOS generate sufficient NO to facilitate essential physiological processes within the wound healing cascade. These processes include forming a protective barrier against microorganisms, increasing microvascular permeability, and stimulating cell proliferation and collagen deposition [7–9]. Similarly, endogenous H_2S is synthesized by three enzymes: cystathionine β-synthase (CBS), cystathionine γ-lyase (CSE), and 3-mercaptopyruvate sulfurtransferase (3-MST). Accumulating evidence indicates that CSE is the predominant enzyme responsible for H_2S production within the vasculature, a process

crucial for wound healing [10]. Many studies have demonstrated that H_2S enhances wound repair through several mechanisms, including proangiogenic, anti-inflammatory, and anti-oxidative. Specifically, H_2S inhibits the secretion of inflammatory mediators, thereby suppressing the early inflammatory response. Additionally, H_2S reduces neutrophil recruitment to the wound site [11,12].

The mechanisms of NO and H_2S in wound healing underscore their therapeutic potential when they are administered independently at appropriate doses and specific sites. Despite the overlapping physiological functions and frequent convergence of similar signaling pathways, NO or H_2S can mutually influence each other's bioavailability and activity [13,14]. Additionally, the interaction between NO and H_2S generates novel signaling molecules, including HNO, HSNO, HSSNO, and RSSH which have distinctive biological effects [15,16].

Accordingly, different types of compounds capable of codelivering NO and H_2S have been developed for the treatment of diseases, including heart failure [17,18], thrombotic disease [19], Alzheimer' disease [20], ischemia-reperfusion injury [21], and so on [22,23]. In our previous work, we constructed an NO and H_2S codelivery system based on an enzyme-prodrug strategy. The controlled release of NO and H_2S exerts a synergistic effect on antithrombosis in both arterial and deep vein thrombosis models [19]. To date, the codelivery systems designed or tested specifically for wound healing are relatively few.

In this study, we first designed and synthesized a novel hybrid prodrug (TSNO) for the codelivery of H_2S and NO under the catalysis of engineered β-galactosidase, and then assessed the release profile of H_2S and NO from the TSNO. Subsequently, TSNO was incorporated into electrospun PCL to fabricate a functional wound dressing. In vivo performance was evaluated in a mouse model of skin wounds; codelivery of H_2S and NO effectively accelerated wound healing (Figure 1). The functional wound dressing represents a promising candidate for treating large-scale skin wounds in the clinic.

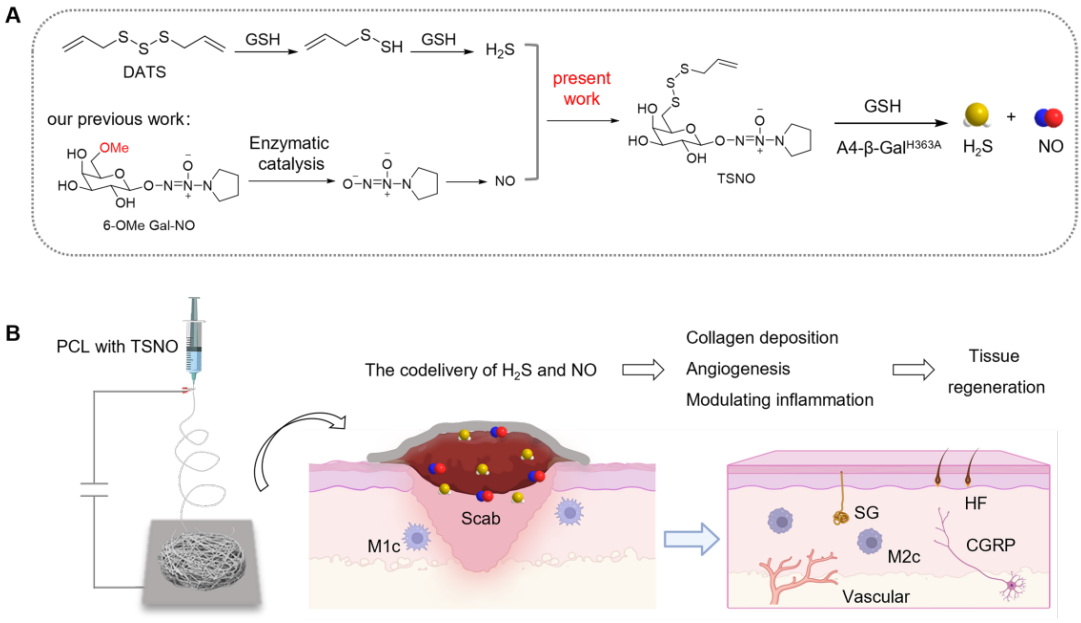

Figure 1. Design and fabrication of the wound dressing with the function of codelivery of H_2S and NO. (**A**) Design of the hybrid prodrug of H_2S and NO (TSNO). (**B**) Schematic illustration showing the fabrication of the functional dressing and its application for the treatment of wound healing.

2. Methods and Materials

2.1. Materials

All chemicals and reagents were of reagent grade commercially obtained and used directly without further purification. Reaction reagents including D-galactose, tosyl chloride, triethylamine were obtained from Shanghai Aladdin Bio-Chem Technology Co., Ltd (Shanghai, China). Potassium thioacetate, 33 wt.% hydrogen bromide solution in acetic acid, prop-2-ene-1-thiol, *N*,*N*′-thiodiphthalimide were ordered from Beijing InnoChem Science & Technology Co., Ltd (Beijing, China). Anhydrous sodium methoxide and methanol were purchased from J&K Scientific (Beijing, China). Anhydrous pyridine, dichloromethane, *N*,*N*-dimethylformamide and acetonitrile were ordered from Meryer Chemical Technology Co., Ltd (Shanghai, China). Ethyl acetate, petroleum ether, dichloromethane, ethanol, methanol, acetone, sulfuric acid, acetic anhydride and acetic acid were purchased from

Tianjin Zhiyuan Chemical Reagent Co., Ltd (Tianjin, China). In addition, inorganic salts like sodium chloride, sodium bicarbonate, sodium hydroxide, and anhydrous sodium sulfate were obtained from Shanghai Macklin Biochemical Co., Ltd (Shanghai, China).

2.2. Synthesis and Characterization of TSNO

The chemical structures of compounds were confirmed by ^{1}H NMR and ^{13}C NMR, recorded on a Bruker Avance-400 FT nuclear magnetic resonance spectrometer. Chemical shifts were reported relative to the reference chemical shift of the NMR solvent. The following splitting abbreviations were used: s = singlet, d = doublet, dd = doublet of doublets, t = triplet, m = multiplet. High-resolution mass spectra (HRMS) were obtained on a Varian QFT-ESI mass spectrometer.

1,2,3,4-di-*O*-isopropylidene-α-d-galactopyranose (Compound **1**)

Compound **1** was synthesized according to the reported procedure [24]. Briefly, galactose (20 g, 110 mmol) was dissolved in dry acetone (500 mL) and concentrated H_2SO_4 (10 mL) was added dropwise to the solution with an ice bath. The mixture was then stirred for 12 h at room temperature. Subsequently, the reaction was neutralized with NaOH and concentrated under reduced pressure. The resulting syrup was redissolved in EA, washed with water, and dried over Na_2SO_4. The organic solvent was removed under reduced pressure to give the crude product, which was purified by chromatography (PE:EA = 2:1) to afford Compound **1** (25 g, 86% yield) as a pale syrup. ^{1}H NMR (400 MHz, $CDCl_3$) δ (ppm) 5.56 (d, J = 4.8 Hz, 1H), 4.61 (d, J = 7.6 Hz, 1H), 4.33 (dd, J_1 = 4.8 Hz, J_2 = 1.2 Hz, 1H), 4.28 (d, J = 8.0 Hz, 1H), 3.89-3.78 (m, 2H), 3.72 (dd, J_1 = 4.8 Hz, J_2 = 11.2 Hz, 1H), 2.88 (s, 1H), 1.53 (s, 3H), 1.45 (s, 3H), 1.34 (s, 6H); ^{13}C NMR (101 MHz, $CDCl_3$) δ (ppm) 109.3, 108.6, 96.2, 71.3, 70.6, 70.5, 68.3, 61.9, 25.9, 25.8, 24.9, 24.3 (Figure S1).

6-*O*-p-toluenesulfonate-1,2,3,4-di-*O*-isopropylidene-α-d-galactopyranose (Compound **2**)

To a stirred solution of compound **1** (15 g, 57.7 mmol) in dry DCM (200 mL) at 0 °C, a solution of tosyl chloride (16 g, 84.2 mmol) in dry DCM (100 mL) was added dropwise. Then, TEA (16 mL, 110 mmol) was added while maintaining the temperature at 0 °C. The mixture was allowed to warm to ambient temperature and stirred for 12 h. After the starting material was consumed (by TLC), the reaction was quenched with water and extracted with DCM. The combined organic phases were dried over Na_2SO_4 and concentrated in vacuo. The crude product was purified by column chromatography, using a gradient from PE to PE:EA = 3:1, yielding the desired compound **2** (12.5 g, 70%) as a white solid. ^{1}H NMR (400 MHz, $CDCl_3$) δ (ppm) 7.82 (d, J = 8.2 Hz, 2H), 7.34 (d, J = 8.2 Hz, 2H), 5.46 (d, J = 4.8 Hz, 1H), 4.60 (dd, J = 7.8, 2.4 Hz, 1H), 4.30 (dd, J = 4.8, 2.4 Hz, 1H), 4.25–4.16 (m, 2H), 4.14–3.97 (m, 2H), 2.45 (s, 3H), 1.51 (s, 3H), 1.35 (s, 3H), 1.32 (s, 3H), 1.29 (s, 3H); ^{13}C NMR (101 MHz, $CDCl_3$) δ (ppm) 144.79, 132.88, 129.78, 128.14, 109.59, 108.95, 96.16, 70.55, 70.44, 70.40, 68.23, 65.90, 26.01, 25.84, 24.94, 24.38, 21.65 (Figure S2).

6-*S*-acetyl-1,2,3,4-di-*O*-isopropylidene-α-d-galactopyranose (Compound **3**)

Compound **2** (10 g, 24.1 mmol) and potassium thioacetate (5.5 g, 48.2 mmol) were dissolved in dry DMF (60 mL). The resulting mixture was stirred at 60 °C for 18 h. The mixture was then quenched with water and extracted with EA. The combined organic phases were dried over Na_2SO_4 and concentrated in vacuo. The crude product was purified by column chromatography, using a gradient from PE to PE:EA = 5:1, yielding the desired compound **3** (6.2 g, 60%) as a yellow syrup. ^{1}H NMR (400 MHz, $CDCl_3$) δ (ppm) 5.51 (d, J = 4.8 Hz, 1H), 4.61 (dd, J = 7.8, 2.4 Hz, 1H), 4.30–4.25 (m, 2H), 3.94–3.75 (m, 1H), 3.17–3.00 (m, 2H), 2.34 (s, 3H), 1.47 (s, 3H), 1.45 (s, 3H), 1.35 (s, 3H), 1.31 (s, 3H); ^{13}C NMR (101 MHz, $CDCl_3$) δ (ppm) 195.74, 109.46, 108.78, 96.54, 72.06, 70.95, 70.53, 66.83, 30.52, 29.70, 25.96, 25.94, 25.00, 24.44 (Figure S3).

1,2,3,4-*O*-tetraacetyl-6-*S*-acetyl-d-galactopyranose (Compound **5**)

Compound **3** (5 g, 15.7 mmol) was dissolved in 10% AcOH aqueous solution (20 mL). The mixture was stirred at reflux. After the reaction was complete (monitored by TLC), the solvent was removed under reduced pressure to afford compound **4** as a yellow syrup. This material was used directly in the next step.

To a solution of crude compound **4** in dry DMF (10 mL) with an ice bath, Ac_2O (6 mL) and pyridine (10 mL) was added. Then, the reaction was allowed to warm to room temperature and stirred overnight. The reaction was then quenched with water and extracted with EA, the combined organic extracts were washed successively with 1 N HCl, saturated $NaHCO_3$ solution, and brine. The organic phase was dried over Na_2SO_4 and concentrated in vacuo. The crude residue was purified by column chromatography (PE:EA = 1:1) to afford compound **5** (5.7 g, 90% yield) as a yellow syrup. ^{1}H NMR (400 MHz, $CDCl_3$) δ (ppm) 5.67 (d, J = 8.4 Hz, 1H), 5.44 (d, J = 2.8 Hz,

1H), 5.37–5.25 (m, 1H), 5.05 (dd, *J* = 10.4, 3.4 Hz, 1H), 3.83 (t, *J* = 7.0 Hz, 1H), 3.21–3.02 (m, 2H), 2.33 (s, 3H), 2.19 (s, 3H), 2.12 (s, 3H), 2.04 (s, 3H), 1.99 (s, 3H); ^{13}C NMR (101 MHz, $CDCl_3$) δ (ppm) 194.28, 170.20, 169.90, 169.39, 168.92, 92.15, 73.16, 70.99, 68.14, 67.82, 66.39, 30.41, 28.19, 20.78, 20.63, 20.51 (Figure S4).

1-bromine 2,3,4-tri-O-acetyl-6-S-acetyl-α-d-galactopyranoside (Compound **6**)

To a solution of compound **5** (1 g, 2.5 mmol) in dry DCM (5 mL) in an ice bath, 33% HBr in acetic acid (10 mL) was added. The mixture was stirred for 30 min at room temperature, then quenched by adding saturated Na_2CO_3 solution. The mixture was extracted with DCM. The combined organic extracts were dried over Na_2SO_4 and concentrated in vacuo. The crude residue was purified by column chromatography (PE:EA = 3:1) to afford compound **6** (0.99 g, 95% yield) as a pale syrup. ^{1}H NMR (400 MHz, $CDCl_3$) δ (ppm) 6.67 (d, *J* = 3.8 Hz, 1H), 5.52 (d, *J* = 2.6 Hz, 1H), 5.36 (dd, *J* = 10.6, 3.2 Hz, 1H), 5.01 (dd, *J* = 10.6, 3.8 Hz, 1H), 4.26 (t, *J* = 7.2 Hz, 1H), 3.17 (dd, *J* = 13.8, 7.2 Hz, 1H), 2.98 (dd, *J* = 13.8, 7.2 Hz, 1H), 2.34 (s, 3H), 2.17 (s, 3H), 2.10 (s, 3H), 2.00 (s, 3H); ^{13}C NMR (101 MHz, $CDCl_3$) δ (ppm) 194.11, 170.12, 170.06, 169.77, 88.25, 72.52, 68.27, 67.79, 67.71, 30.46, 27.85, 20.76, 20.65, 20.60 (Figure S5).

2,3,4-tri-*O*-acetyl-6-S-acetyl-β-galactopyranosyl-pyrrolidinyl diazeniumdiolate (Compound **7**)

Compound **6** (1 g, 2.3 mmol) and PYRRO/NO (0.52 g, 3.4 mmol) were dissolved in dry CH_3CN (30 mL) under an argon atmosphere. The resulting mixture was stirred at 0 °C for 24. After the reaction was complete, the solvent was removed under reduced pressure. The residue was purified by column chromatography (PE:EA = 1:1) to afford the desired compound **7** (0.73 g, 65% yield) as a yellow solid. ^{1}H NMR (400 MHz, $CDCl_3$) δ (ppm) 5.52 (dd, *J* = 10.2, 8.4 Hz, 1H), 5.41 (d, *J* = 3.2 Hz, 1H), 5.13 (d, *J* = 8.4 Hz, 1H), 5.08 (dd, *J* = 10.2, 3.2 Hz, 1H), 4.21–4.09 (m, 3H), 3.65–3.57 (m, 4H), 2.15 (s, 3H), 2.05 (s, 6H), 2.00 (s, 3H), 1.99–1.93 (m, 4H); ^{13}C NMR (101 MHz, $CDCl_3$) δ (ppm) 170.38, 170.18, 170.09, 169.11, 100.88, 71.30, 71.10, 66.88, 66.77, 61.14, 50.65, 23.03, 20.71, 20.67, 20.61, 20.54 (Figure S6).

6-sulfhydryl-β-galactopyranosyl-pyrrolidinyl diazeniumdiolate (SNO)

To a solution of compound **7** (500 mg, 1.05 mmol) in dry MeOH (15 mL), catalytic amount of MeONa was added. After the reaction was complete, the solvent was concentrated under reduced pressure. The crude product was purified by column chromatography with a gradient elution of MeOH in DCM (from 1% to 5%) to afford the desired compound **SNO** (311 mg, 80% yield) as a white solid. ^{1}H NMR (400 MHz, MeOD) δ (ppm) 4.90 (d, *J* = 8.2 Hz, 1H), 3.99 (d, *J* = 3.2 Hz, 1H), 3.81–3.69 (m, 1H), 3.62–3.58 (m, 2H), 3.57–3.51 (m, 4H), 2.82–2.68 (m, 2H), 2.04–1.88 (m, 4H); ^{13}C NMR (101 MHz, MeOD) δ (ppm) 103.80, 77.35, 73.42, 68.95, 68.36, 50.52, 23.45, 22.42 (Figure S7).

2-(allyldisulfaneyl) isoindoline-1,3-dione (Compound **8**)

A solution of 2-propene-1-thiol (1 g, 13.4 mmol) and *N,N'*-thiodiphthalimide (6.5 g, 20.2 mmol) in 1,2-dichloroethane (50 mL) was stirred at 83 °C for 4 h. After completion of the reaction (monitored by TLC), the mixture was cooled to 0 °C in an ice bath. The byproduct was removed by filtration, and the filtrate was concentrated in vacuo. The crude residue was purified by column chromatography (PE:EA = 20:1) to afford the desired product **8** (3 g, 88% yield) as a white solid. ^{1}H NMR (400 MHz, $CDCl_3$) δ (ppm) 7.94 (dd, *J* = 5.6, 3.2 Hz, 2H), 7.80 (dd, *J* = 5.6, 3.2 Hz, 2H), 5.91 (dd, *J* = 17.0, 9.8 Hz, 1H), 5.42 (dd, *J* = 17.0, 1.2 Hz, 1H), 5.30–5.18 (m, 1H), 3.70 (d, *J* = 4.2 Hz, 2H); ^{13}C NMR (101 MHz, $CDCl_3$) δ (ppm) 167.65, 134.87, 132.23, 132.20, 124.05, 119.85, 43.85 (Figure S8).

6-allyltrisulfanyl-β-galactopyranosyl-pyrrolidinyl diazeniumdiolate (TSNO)

Compound **SNO** (0.1 g, 0.32 mmol) and compound **8** (97 mg, 0.38 mmol) were dissolved in dry DCM (10 mL). The mixture was stirred for 6 h at room temperature. After the reaction was complete, the solvent was concentrated under reduced pressure. The residue was purified by column chromatography with a gradient elution of MeOH in DCM (from 1% to 4%) to afford the desired compound **TSNO** (120 mg, 90% yield) as a white solid. ^{1}H NMR (400 MHz, $CDCl_3$) δ (ppm) 5.88 (ddt, *J* = 17.2, 9.8, 7.2 Hz, 1H), 5.34–5.11 (m, 2H), 4.96 (d, *J* = 8.2 Hz, 1H), 4.19–4.09 (m, 1H), 4.04 (dd, *J* = 9.8, 8.2 Hz, 1H), 3.93 (t, *J* = 6.8 Hz, 1H), 3.77 (dd, *J* = 9.8, 3.2 Hz, 1H), 3.58 (td, *J* = 6.2, 3.2 Hz, 4H), 3.51 (dt, *J* = 7.4, 1.0 Hz, 2H), 3.30–3.14 (m, 2H), 2.05–1.82 (m, 4H); ^{13}C NMR (101 MHz, $CDCl_3$) δ (ppm) 132.78, 119.27, 103.56, 73.67, 73.51, 68.99, 68.93, 50.82, 41.38, 38.81, 23.03. HRMS (m/z): $[M + NH_4]^+$ calcd. for $C_{13}H_{23}N_3O_6S_3$, 431.1093; found, 431.1087 (Figure S9).

2.3. Molecular Docking

The 3D structures of galactose and 6-SH galactose were drawn using chemdraw 3D. Energy minimization was performed before docking. Homology modeling of A4-β-Gal^{H363A} was done using Swiss-Model, with the X-ray crystal structure of A4-β-Gal (PDB: 1KWK) as a template. The highest-scoring crystal structure was selected. Docking center of A4-β-Gal^{H363A} was set at x = 24, y = 10, z = 28, with a box size of x = 40, y = 40, z = 40, based on the binding site of A4-β-Gal. The conformation with the lowest free energy was used to determine the optimal binding mode.

2.4. Expression and Purification of A4-β-Gal^{H363A}

Both A4-β-Gal and A4-β-Gal^{H363A} were cloned into the pET22b(+) vector for expression as recombinant proteins and were expressed in E. *coli* BL21(DE3) as described in our previous work [25]. Briefly, E. *coli* BL21(DE3) strains were cultured in LB medium supplemented with ampicillin (100 μg/mL) at 37 °C with shaking at 220 rpm for 4 h. Then, 0.1 mM isopropyl-β-D-thiogalactopyranoside (IPTG) was added to the culture, and the culture was incubated at 18 °C with shaking at 180 rpm for 24 h. The *E. coli* were harvested by centrifugation and lysed by sonication; the supernatant was then obtained by centrifugation (12,000 rpm, 4 °C, 30 min). The supernatant was then loaded onto a Ni^{2+}-NTA affinity column (Qiagen, Hilden, Germany) to purify the target protein. Elution fractions were analyzed using SDS-PAGE followed by Coomassie blue staining. Protein concentration was determined using a BCA Protein Assay Kit (Pierce Biotechnology, Rockford, IL).

2.5. Measurement of NO Release

The *in vitro* release of NO from SNO or TSNO was assessed using a Griess assay kit. Specifically, 100 μM of the NO donor was dissolved in PBS (pH 7.4) and co-incubated with A4-β-Gal^{H363A} (0.005 mg/mL) and GSH (at concentrations of 1 mM, 100 μM, and 10 μM) at 37 °C. At each predetermined time point, 50 μL of the reaction mixture was collected and transferred to a 96-well plate. Subsequently, 50 μL of Griess reagent I and 50 μL of Griess reagent II were added. Absorbance was measured at 540 nm using an Enspire microplate reader (PerkinElmer LLC, MA, USA). The concentration of NO was calculated using a $NaNO_2$ standard curve.

In vitro NO release from TSNO was further detected using an NO-sensitive electrode (WPI) at room temperature. A solution of TSNO (1 μM) in PBS buffer (pH 7.4) was prepared. The NO electrode was immersed, and the baseline was stabilized. Subsequently, 100 μL of A4-β-Gal^{H363A} enzyme solution (0.005 mg/mL) and 100 μL of GSH (1 mM) were added to the solution. Data was collected using the recording system (WPI).

2.6. Measurement of H_2S Release

The in vitro release of H_2S from TSNO was determined by the Methylene blue (MB) assay. Specifically, 100 μM TSNO was dissolved in PBS (pH 7.4) and co-incubated with GSH (at concentrations of 1 mM, 100 μM, and 10 μM) at 37 °C. At each predetermined time point, 100 μL of the reaction mixture was collected and transferred to a 96-well plate. Subsequently, 20 μL of zinc acetate (1%, *w*/*v*), 40 μL of $FeCl_3$ (30 mM in 1.2 M HCl), and 40 μL of *N,N*-dimethyl-p-phenylene diamine (20 mM in 7.2 M HCl) were added. Absorbance was measured at 670 nm using an Enspire microplate reader (PerkinElmer LLC, MA, USA). The concentration of H_2S was calculated using a NaHS standard curve.

In vitro H_2S release from TSNO was further detected using an H_2S-sensitive electrode (WPI) at room temperature. A solution of TSNO (1 μM) in PBS buffer (pH 7.4) was prepared. The H_2S electrode was immersed, and the baseline was stabilized. Subsequently, 100 μL of GSH (1 mM) were added to the solution. Data was collected using the recording system (WPI).

2.7. Cell Proliferation Assay

Human umbilical vein endothelial cells (HUVECs) were purchased from American Type Culture Collection (Rockville, MD, USA). HUVECs were maintained in Endothelial Growth Medium-2 (EGM-2; Lonza, Walkersville, MD, USA). Cells were cultured at 37 °C in a humidified atmosphere containing 5% CO_2 and passaged every other day using 0.05% trypsin-EDTA (Gibco Life Sciences, Grand Island, NE, USA), with a split ratio of 1:2.

Cells were seeded at a density of 1000 cells/well in 100 μL of media into 96-well plates and treated with 10 μM TSNO under different conditions. For the Cell Counting Kit-8 (CCK-8) assay, after 1 and 2 days of incubation, CCK-8 solution was added to each well. The optical density (OD) at 450 nm was measured using a microplate reader (BioRad). For the Crystal Violet Staining, after 2 days of incubation, cells were fixed by adding 100 μL of ice-cold

glutaraldehyde (1.1% in PBS) to each well. After washing with PBS, 100 μL of 0.1% crystal violet solution was added to each well for 20 min at room temperature, images of stained cells were acquired using a microscope.

2.8. Scratch Wound-Healing Assay

HUVECs were seeded in 6-well plates. When cells reached confluence, scratch wounds were generated across each well using a sterile plastic 10 μL micropipette tip. After washing cells twice with PBS and treated with 10 μM TSNO under different conditions. Images from three randomly selected fields per scratch were captured at 0 and 9 h under a microscope. The migration was quantified by measuring the number of migrated cells in the wound area using Image J software (v1.53, 2023).

2.9. Fabrication and Characterization of Wound Dressing

Electrospinning was performed using a climate-controlled electrospinner. Briefly, PCL (80 K) and TSNO (1 mg/mL) were dissolved in chloroform/methanol (5:1 *v*/*v*) and stirred vigorously to form a homogeneous solution with a final polymer concentration of 20 wt.% (*w*/*v*). Mats were fabricated under these parameters: needle-to-collector distance = 15 cm, flow rate = 4 mL/h, and applied voltage = 12 kV. The as-prepared mats were vacuum-dried at room temperature to ensure complete solvent removal.

The surface morphology of electrospun mats was observed using a field emission scanning electron microscope (SEM; FEI Quanta 200, Prague, Czech Republic) at an accelerating voltage of 10 kV. The surface was sputter-coated with gold before observation.

Tensile testing of the electrospun mats was performed using an Instron universal tensile tester (model 5865) at ambient temperature and a crosshead speed of 10 mm/min. Rectangular specimens (15 × 10 × ~0.4 mm) were prepared, and a gauge length of 10 mm was employed.

2.10. Skin Wound Model

The use of experimental animals has been approved by the Animal Experiment Ethics Committee of Nankai University, and the operations were conducted in accordance with the Guide for the Care and Use of Laboratory Animals. The method for establishing the mouse skin wound model refers to previous descriptions [26]. The specific steps are as follows: C57BL/6J mice (male, 8 weeks old) were selected and anesthetized by intraperitoneal injection of sodium pentobarbital (30 mg/kg) before surgery. After shaving the mice, a full-thickness excised skin wound (size: 1 cm × 1 cm) was created on their backs. The mice were randomly divided into 5 groups, including the PBS group, PCL patch group, NO patch group, H_2S patch group, and NO-H_2S patch group (n = 4 in each group). The patches in the patch groups were fixed on the wound surface by suture. The corresponding enzyme solution for each prodrug was regularly applied to the patch site every 3 days to achieve the delivery purpose. The scar edge and wound area were measured accordingly. The wound area percentage = A/A1 × 100, where A1 represents the area on day 1, and A represents the area at a specific time point. On day 14 after surgery, the mice were sacrificed and skin samples were collected for subsequent experiments.

2.11. Histological Analysis

To observe wound healing and scar formation, skin tissue samples were collected on the 14th day after surgery. The samples were fixed in 4% paraformaldehyde for 30 min, washed with PBS, and then dehydrated in 30% sucrose overnight. Afterwards, the skin tissue samples were embedded in OCT and cut into 6 μm-thick sections. Hematoxylin-eosin (H&E) staining, Masson's trichrome staining, and Sirius red staining were used for histological analysis. All the above three staining kits were purchased from Leagene Biotechnology Co., Ltd., Beijing, China. Images were observed using an upright microscope (Ernst Leitz GmbH, Wetzlar, Germany) and analyzed with ImageJ software.

The procedure for immunofluorescence staining was as follows: A series of primary antibodies were used, including anti-CD31 (BD Pharmingen, 1:100), anti-α-SMA (Abcam, 1:100), anti-CD68 (Abcam, 1:100), anti-iNOS (Abcam, 1:100), anti-CD206 (Abcam, 1:100), and anti-CGRP (Abclonal, 1:100). The secondary antibodies used were rhodamine-labeled or fluorescein isothiocyanate (FITC)-labeled goat anti-mouse IgG (1:200, Invitrogen), rhodamine-labeled or FITC-labeled goat anti-rabbit IgG (1:200, Invitrogen) and rhodamine-labeled goat anti-rat IgG (1:200, Invitrogen). For in situ superoxide imaging using DHE (Dihydroethidium) fluorescent probe (MCE), frozen sections were incubated with DHE probe in PBS at 37 °C for 30 min in a light-protected and humidified incubation box, followed by three washes with PBS. Sections incubated with secondary antibodies without primary antibodies served as negative controls. The nuclei were counterstained using a mounting medium

containing 4,6-diamidino-2-phenylindole (Southern Biotechnology Associates, Inc., Birmingham, AL, USA). Images were observed using a fluorescence microscope (Zeiss Axio Imager Z1, Carl Zeiss AG, Baden-Wuerttemberg, Germany) and analyzed with ImageJ software.

2.12. Quantitative Real-Time Polymerase Chain Reaction (RT-qPCR)

Tissue samples were ground in liquid nitrogen, and total RNA was extracted using TRIzol reagent (Invitrogen). Subsequently, total RNA was reverse-transcribed into cDNA with Hifair® III 1st Strand cDNA Synthesis SuperMix for qPCR (gDNA digester plus) (Yeasen). Quantitative analysis of the expression levels of related genes was performed using real-time polymerase chain reaction (Bio–Rad) combined with Hieff® qPCR SYBR Green Master Mix (No Rox) (Yeasen). The relative expression level of the target gene mRNA was expressed as $2^{-(\triangle\triangle CT)}$, and normalized with GAPDH as the internal reference. The primer sequences used in this study are listed in Table S1.

2.13. Statistical Analysis

All data expressed as the mean ± sem were analyzed using GraphPad Prism 8 software with one-way ANOVA followed by Tukey's post-hoc analysis. Differences were considered to be significant at p value < 0.05.

3. Results and Discussion

3.1. Synthesis of the Hybrid Prodrug of H_2S and NO (TSNO)

DATS, an organic polysulfide derived from garlic, can produce H_2S through nucleophilic substitution by GSH at the α-carbon of the allyl substituent, followed by a thiol-disulfide exchange that releases H_2S [27]. For controlled NO release, our previous study reported a precise NO delivery system based on MeGal-NO [25,28], which was synthesized by introducing a methyl group at the O6 position of Gal-NO, and is specifically recognized by the engineered enzyme. From a reaction mechanism point of view, in this work, we designed a novel H_2S and NO dual-donor molecule **TSNO**, by replacing the 6-methyl group with an allyl trisulfide group at the O6 position (Figure 1A).

TSNO is synthesized via a multistep reaction, as illustrated in Figure 2. Briefly, to enable selective modification at the O6 position of galactose, acetone is employed to protect the hydroxyl groups at other positions via Ketalization [29], affording compound **1**. O-Tosylation at the O6 position yields intermediate **2**, which was further thioacetylated using potassium thioacetate as a reagent to yield **3**. The protecting groups in **3** were removed via acetic acid catalyzed hydrolysis, followed by acetylation to form **5**. Subsequently, compound **5** was reacted with hydrobromic acid to obtain **6**. Condensation of **6** with PYRRO/NONOate resulted in **7**, which was deacetylated by sodium methoxide to afford **SNO**. Compound **8** was synthesized via a thiol exchange reaction between 2-propene-1-thiol and *N,N′*-thiodiphthalimide. Finally, the target compound **TSNO** was obtained by reacting **SNO** with **8** via an additional thiol exchange reaction. All compounds were characterized by NMR spectroscopy (^{1}H and ^{13}C), and **TSNO** was additionally confirmed by HRMS.

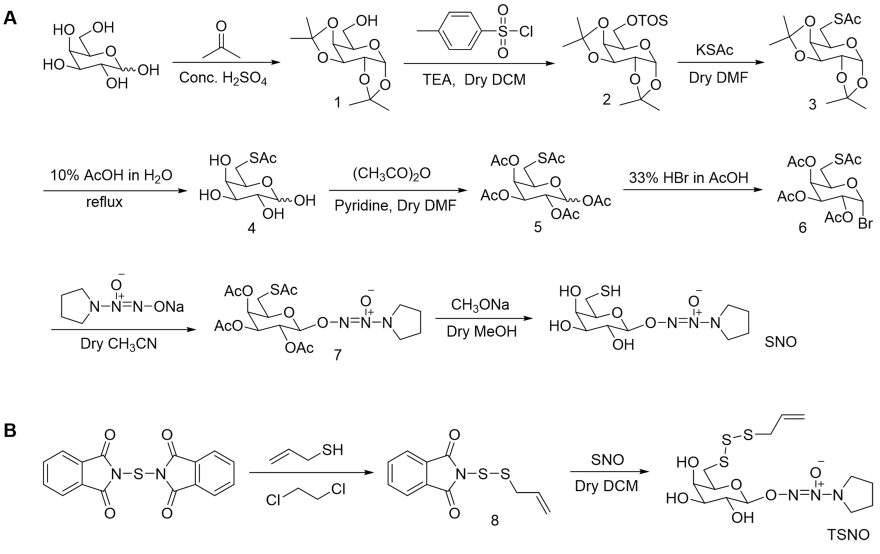

Figure 2. Synthesis of the hybrid prodrug of H_2S and NO (TSNO). (**A**) Synthesis of the SNO. (**B**) Synthesis of the TSNO.

3.2. Engineering A4-β-Gal^{H363A} for Activating TSNO-Prodrug

To screen mutant enzymes capable of specifically hydrolyzing the substrate to release NO, molecular docking was first performed (Figure 3A,B). Docking 6-SH Gal into A4-β-Gal indicated that the 6-SH group could not be accommodated within the pocket due to steric clashes. Based on the "bump-and-hole" principle, we previously engineered an enzyme A4-β-Gal^{H363A} through replacing His363 with a small alanine residue [25]. Interestingly, docking 6-SH Gal into the active pocket of A4-β-Gal^{H363A} demonstrated that the 6-SH group was also well accommodated within the expanded pocket. However, docking 6-allyl trisulfide Gal into A4-β-Gal^{H363A} was unsuccessful due to steric and cavity complementarity mismatches caused by the allyl trisulfide moiety.

Furthermore, both the A4-β-Gal and A4-β-Gal^{H363A} proteins were successfully expressed by *E. coli* BL21 (DE3) cells and purified using nickel-nitrilotriacetic acid (Ni-NTA) affinity chromatography, as confirmed by sodium dodecyl sulfate-polyacrylamide gel electrophoresis (SDS-PAGE) (Figure 3C). In vitro NO release from SNO and TSNO in response to either A4-β-Gal or engineered A4-β-Gal^{H363A} was measured by Griess assay. As shown in Figure 3D, both TSNO and SNO were stable, and no release was detected in the presence of A4-β-Gal. However, incubation of SNO with A4-β-Gal^{H363A} resulted in notable and continuous NO release. In contrast, incubation of TSNO with A4-β-Gal^{H363A} yielded no detectable NO generation.

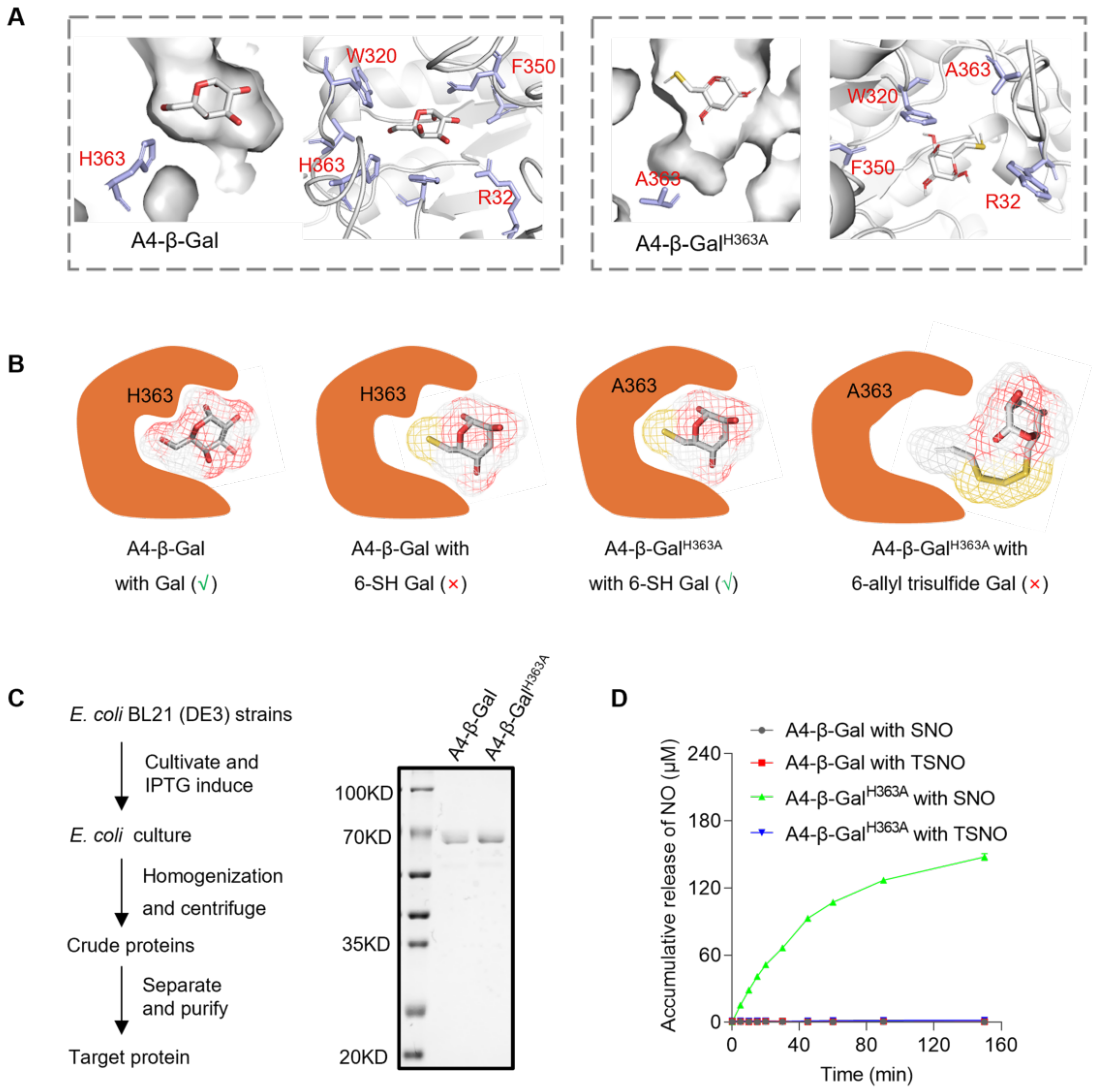

Figure 3. Expression and evaluation of engineered A4-β-Gal^{H363A}. (**A**) Active sites are shown of the wild-type A4-β-Gal (PDB ID: 1KWK, **left**) and the engineered A4-β-Gal^{H363A}. 6-SH Gal was docked into the active pocket of A4-β-Gal^{H363A} using Autodock vina (**right**). (**B**) Schematic illustrations depicting Gal, 6-SH Gal, and 6-allyl trisulfide Galdocked with A4-β-Gal or the engineered A4-β-Gal^{H363A} mutant. (**C**) Shown is the process of expression and purification of the engineered A4-β-Gal^{H363A}. (**D**) In vitro NO release from SNO and TSNO in response to either the A4-β-Gal or engineered A4-β-Gal^{H363A} measured by Griess assay (n = 3).

3.3. In vitro release of H_2S and NO from the TSNO prodrug

On the basis of the structure of TSNO, it is supposed to release H_2S and NO via two steps. Initially, the organic polysulfide moiety can produce H_2S through nucleophilic substitution by a thiol at the α-carbon of the allyl substituent, followed by a thiol-disulfide exchange that could release H_2S. Subsequently, NO will release from the residual SNO structure under the catalysis of the engineered enzyme A4-β-Gal^{H363A} (Figure 4A). On the other hand, TSNO is stable in the presence of A4-β-Gal^{H363A} due to a steric clash between its bulky moiety and the active site. In vitro release of H_2S and NO from the TSNO was investigated by methylene blue and Griess assays, respectively. First, the release of H_2S from TSNO was tested with various thiol catalysts. Although both GSH and Cys showed catalytic efficacy (Figure S10A), GSH demonstrated superior activity, therefore it was chosen for all further experiments. As shown in Figure 4B, TSNO was stable with no obvious H_2S release in PBS (pH 7.4). Upon exposure of TSNO to GSH, H_2S release was clearly observed. As expected, H_2S release increased with increasing GSH concentration. Similarly, TSNO remained stable in the presence of A4-β-Gal^{H363A}, whereas the release of NO was initiated upon treatment with both A4-β-Gal^{H363A} and GSH (Figure 4C). The release of H_2S and NO from TSNO was also measured at various pH values, and similar release profiles were observed (Figure S10B,C). Furthermore, H_2S and NO production from TSNO was directly detected using an H_2S- or NO-sensitive electrode. When incubated with an H_2S-sensitive electrode, TSNO did not generate any measurable signal. In contrast, marked measurable electrical signals were immediately observed following the addition of GSH (Figure 4D). Similarly, NO signals were detected in the presence of both A4-β-Gal^{H363A} and GSH (Figure 4E).

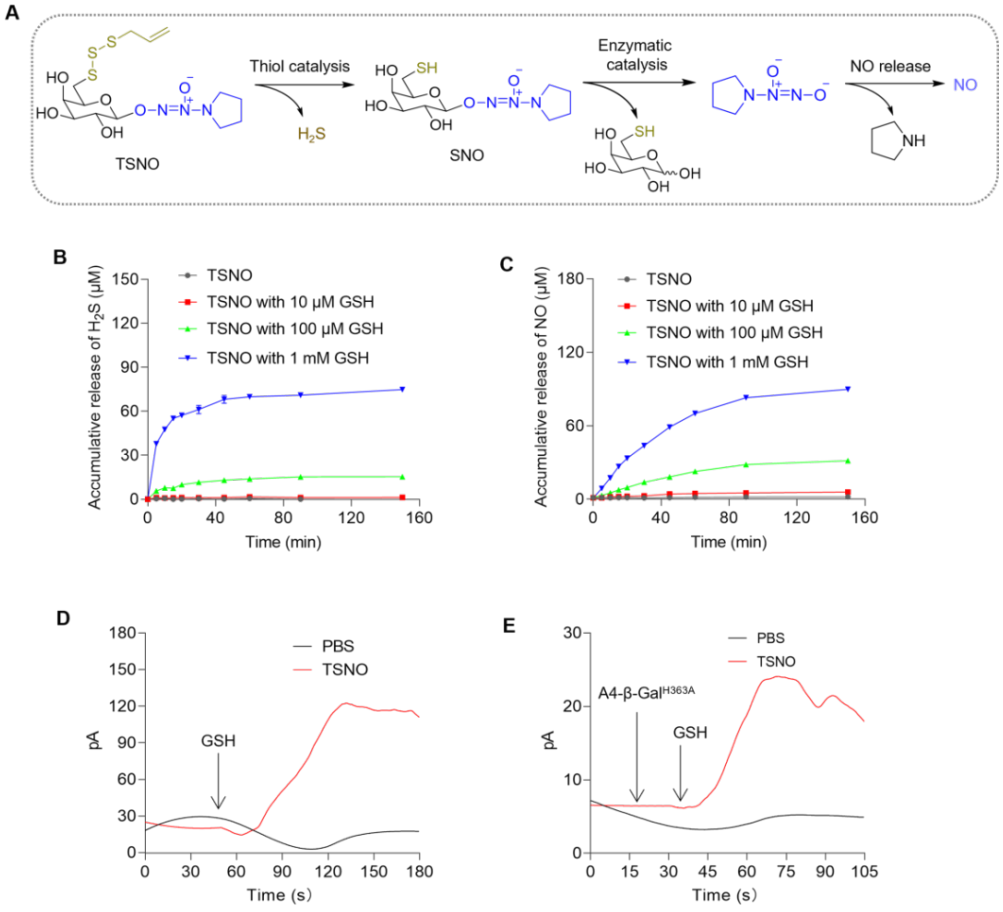

Figure 4. In vitro release of H_2S and NO from the TSNO prodrug. (**A**) Schematic illustration showing the release of H_2S and NO from the TSNO prodrug. (**B**) In vitro release of H_2S from the TSNO prodrug in the presence of GSH (n = 3). (**C**) In vitro release of NO from the TSNO prodrug in the presence of GSH and engineered A4-β-Gal^{H363A} (0.005 mg/mL) (n = 3). (**D**) Real-time monitoring of H_2S release from the TSNO prodrug by an H_2S electrode (WPI). (**E**) Real-time monitoring of NO release from the TSNO prodrug by an NO electrode (WPI).

3.4. Codelivery of H_2S and NO Promotes Endothelial Cell Proliferation and Migration In Vitro

Angiogenesis has been accepted as a prerequisite for wound healing [30]. To investigate the effect of the codelivery of H_2S and NO from TSNO prodrug on angiogenesis, the proliferation of HUVECs were performed.

Both H_2S and NO individually promoted the proliferation of HUVEC compared to the control group; a more pronounced effect on cell proliferation was observed when H_2S and NO were administered in combination with TSNO, as evidenced by both CCK8 assay (Figure 5A,B) and crystal violet staining (Figure 5C). In addition, the synergistic effect of H_2S and NO on the migration of HUVECs was evaluated using a wound scratch assay. As shown in Figure 5D, codelivery of H_2S and NO enhanced cell migration, resulting in smaller scratch widths than those in the control group. Statistical analysis further confirmed that H_2S and NO synergistically promoted cell migration (Figure 5E).

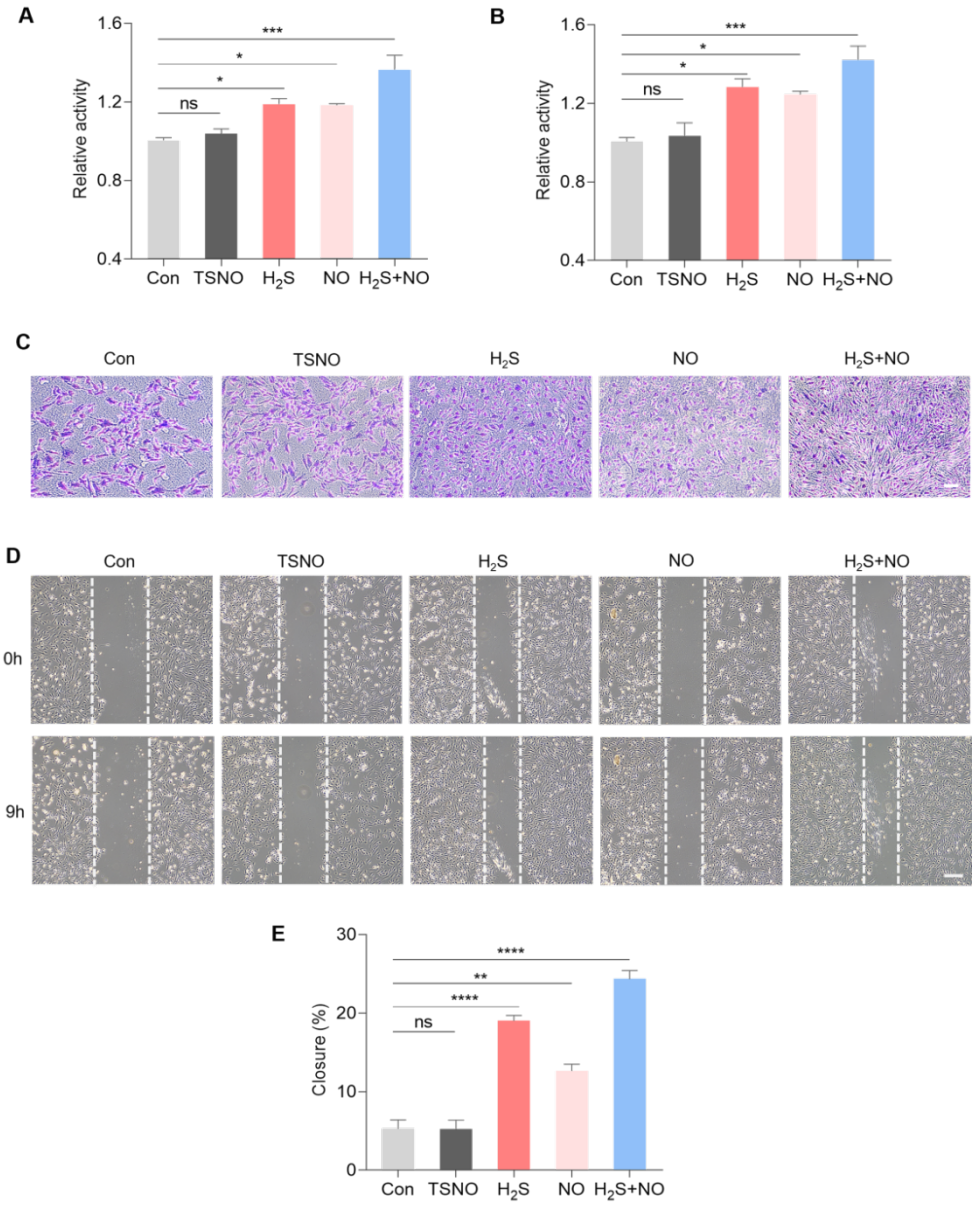

Figure 5. Codelivery of H_2S and NO from the TSNO prodrug synergistically promoted the proliferation and migration of HUVECs. (**A**,**B**) CCK-8 assessment for the proliferation of HUVECs after different treatments at 1 (**A**) and 2 days (**B**). (**C**) Representative images of the crystal violet staining for HUVECs after different treatments at 2 days. Scale bar, 100 μm. (**D**) Representative images of the scratch wound assay for HUVECs after different treatments. Scale bar, 200 μm. (**E**) The quantitative analysis of closure ratio in each group at 9 h. Statistical significance was assessed by One-way ANOVA with Tukey's post-hoc analysis. Data are presented as the means ± SEM, n = 3 per group. * $p < 0.05$, ** $p < 0.01$, *** $p < 0.001$ and **** $p < 0.0001$. ns, not significant.

3.5. Codelivery of H_2S and NO Enhances Wound Healing in a Mouse Model

To evaluate the therapeutic potential of the H_2S and NO codelivery system in tissue repair and regeneration, we established a mouse model of full-thickness skin wounds. A fibrous mat was prepared by electrospinning of PCL loaded with various prodrugs. Scanning electron microscopic (SEM) images showed a homogeneous

structure, and tensile testing indicated that the mat show optimal mechanical properties for the application of wound dressing (Figure S11). The mat was transplanted to the dorsal skin wound sites, and a solution of GSH and engineered enzyme was administered to catalyze the release of H_2S and NO from the prodrug (Figure 6A). The wound closure rate was determined on the basis of the wound area eliminated the impact of differences in initial size, and the result indicates that the codelivery of H_2S and NO exhibited superior efficacy in promoting skin healing compared with that in the other groups (Figure 6B).

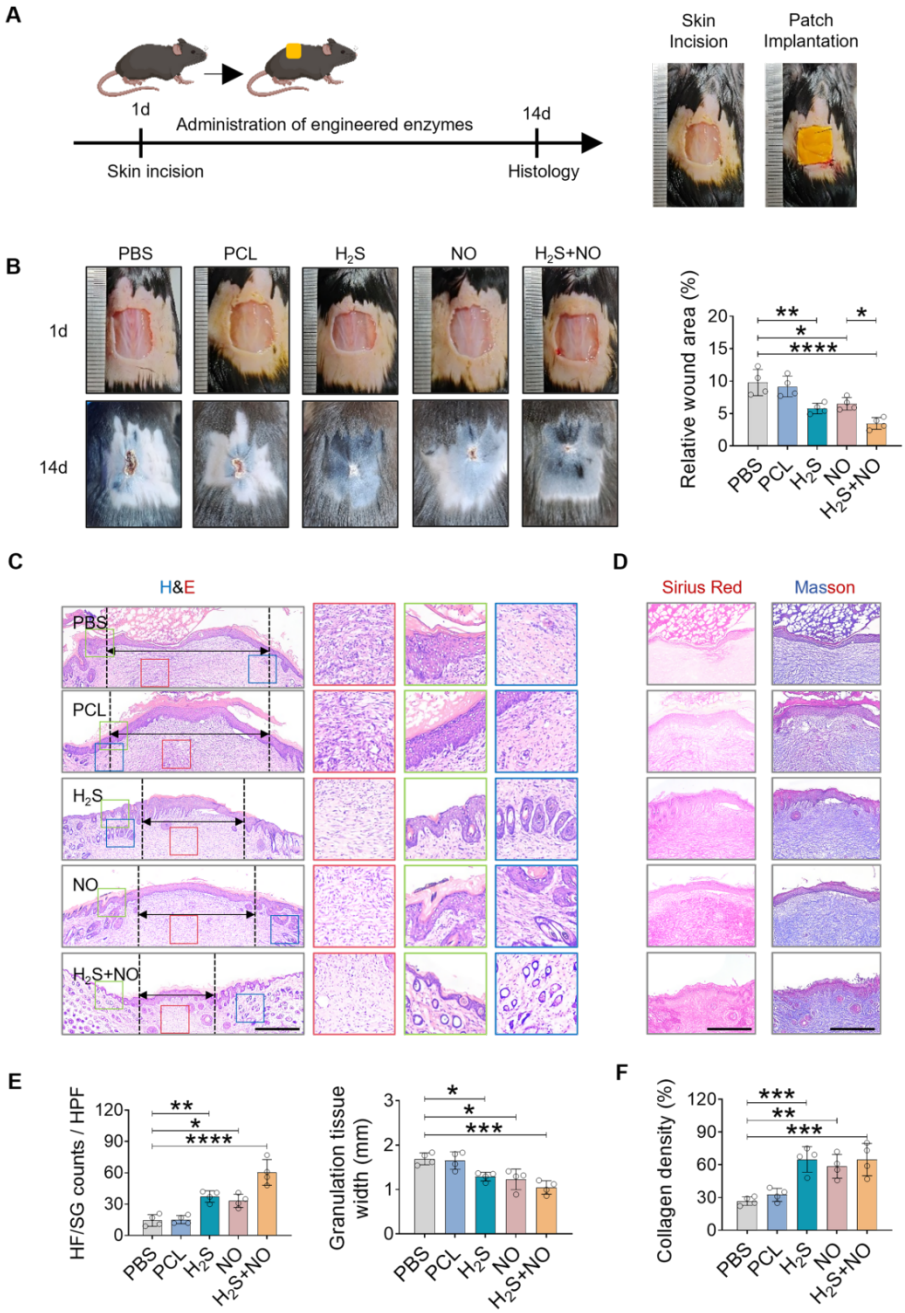

Figure 6. Codelivery of H_2S and NO by the TSNO-loaded wound dressing enhances skin healing in a large full-thickness excisional wound model. (**A**) Experimental schedule for the treatment of full-thickness excisional wound by the TSNO-loaded wound dressing. (**B**) Representative images of wound healing appearance and the quantification of wound closure rate after different treatments. (**C**) H&E staining of wound tissues after different treatments at 14 days. Scale bar, 500 μm. (**D**) Sirius red and masson's trichrome staining of wound tissues after different treatments at 14 days. Scale bar, 500 μm. (**E**) The quantitative analysis of relative granulation tissue width and HF/SG counts in wound areas from (**C**). (**F**) The quantitative analysis of collagen density in wound areas from (**D**). Statistical significance was assessed by One-way ANOVA with Tukey's post-hoc analysis. Data are presented as the means ± SEM, n = 4. * $p < 0.05$, ** $p < 0.01$, *** $p < 0.001$ and **** $p < 0.0001$.

Furthermore, histological analysis by H&E staining revealed the presence of residual scab structures in both the PBS and PCL groups, reflecting the poor healing. In contrast, improved healing was observed in the group treated with H_2S or NO alone. Notably, the H_2S-NO group displayed the most pronounced effect, as demonstrated by a smaller granulation tissue area along with abundant hair follicles and sweat gland tissues (Figure 6C,E). Given that collagen fiber formation is critical for skin tissue healing, Sirius red and Masson's staining were performed and the results supported the enhanced collagen deposition in damaged tissues after treatment with H_2S and NO, alone or in combination (Figure 6D,F).

These findings indicate that codelivery of H_2S and NO effectively enhances the repair and regeneration of damaged skin tissue, with newly formed skin possessing more intact functional units including hair follicles and sweat glands [31]. Mechanistically, enhanced collagen formation by the combination of H_2S and NO provides a structural support to newly formed skin, facilitating tissue remodeling and strength recovery, thereby improving the integrity of skin function accordingly.

3.6. H_2S and NO Cooperatively Promote Angiogenesis and CGRP Release

Angiogenesis is a pivotal biological process in wound healing and repair, as it supports tissue remodeling and functional recovery by supplying oxygen and nutrients to sustain cellular metabolism, thus promoting cell migration and accelerating re-epithelialization [32]. H_2S and NO can promote angiogenesis either independently or synergistically [5,33]. In this study, we found that both H_2S and NO markedly promoted angiogenesis and significantly ($p < 0.005$) increased the number of $CD31^+$ blood vessels compared with that in the control group (PBS) (Figure 7A). Immunofluorescence staining for α-SMA revealed that H_2S and NO cooperatively promoted the formation of small arterioles at the wound site (Figure 7B). The upregulated expression of angiogenesis-related genes further confirmed that the combination of H_2S and NO is more effective in facilitating angiogenesis in damaged tissues than other treatments (Figure 7D).

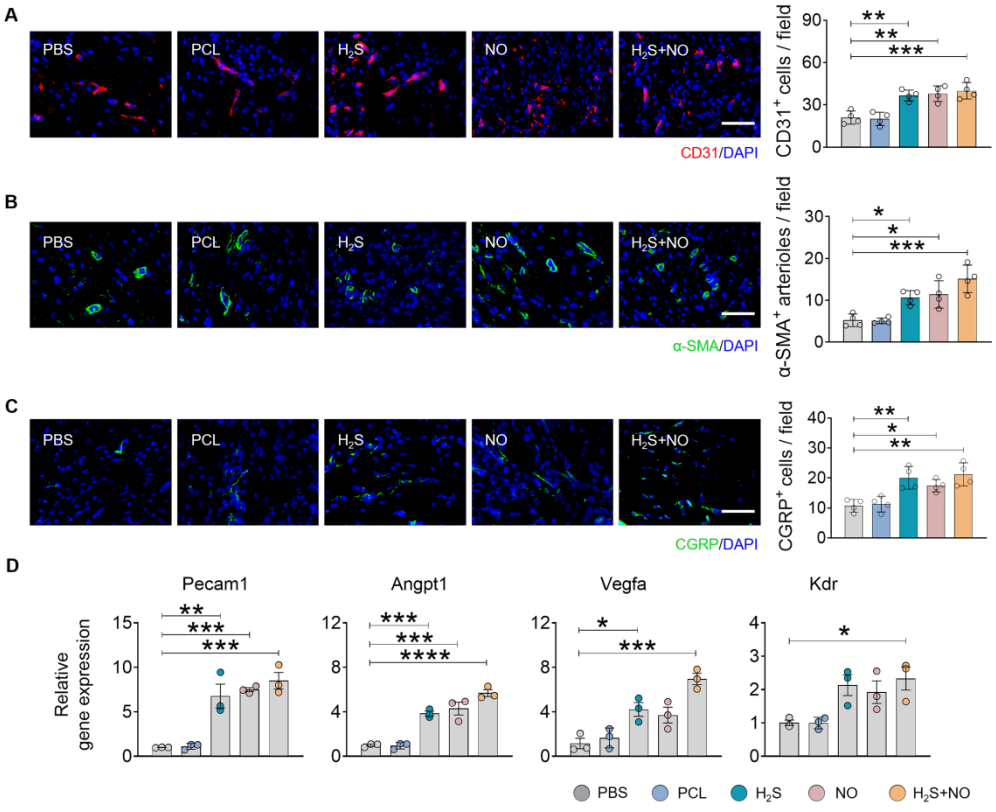

Figure 7. H_2S and NO cooperatively promotes angiogenesis and CGRP release in wound areas. (**A**) Immunofluorescence staining for CD31 with the quantification of $CD31^+$ cells in wound areas (n = 4). Scale bar, 50 μm. (**B**) Immunofluorescence staining for α-SMA with the quantification of $\alpha\text{-SMA}^+$ arterioles in wound areas (n = 4). Scale bar, 50 μm. (**C**) Immunofluorescence staining for CGRP with the quantification of $CGRP^+$ cells in wound areas (n = 4). Scale bar, 50 μm. (**D**) The relative expression of angiogenesis-related genes by RT–qPCR assay (n = 3). Statistical significance was assessed by One-way ANOVA with Tukey's post-hoc analysis. Data are presented as the means ± SEM. * $p < 0.05$, ** $p < 0.01$, *** $p < 0.001$ and **** $p < 0.0001$.

It has been accepted that H_2S and NO can react in vivo to generate HNO [34], which activates neuroendocrine signaling pathways and promotes the release of calcitonin gene-related peptide (CGRP), a neuropeptide widely distributed in the nervous system and peripheral tissues [35]. In addition, the critical role of CGRP in skin wound healing and regeneration has recently been highlighted [36]. Herein, an HNO-specific fluorescence probe was employed to detect the generation of HNO due to the interaction between H_2S and NO. A marked fluorescence signal was observed in the H_2S-NO group compared to the other groups (Figure S12). And the immunofluorescence staining revealed that the treatment with H_2S and NO, alone or in combination, also increased CGRP production (Figure 7C).

3.7. H_2S and NO Cooperatively Inhibit Oxidative Stress and Modulate Inflammation in Wound Areas

Oxidative stress and inflammatory responses are involved throughout the entire tissue healing process [37]. DHE staining first demonstrated that both H_2S and NO effectively inhibited ROS production (Figure 8A). Immunofluorescence staining for CD68 revealed that H_2S and NO also suppressed macrophage infiltration in wound tissues (Figure 8B). More importantly, we found that codelivery of H_2S and NO reduced the number of proinflammatory M1 macrophages while increasing the number of M2 macrophages, a subset known to play a key role in tissue repair and regeneration, compared with the other groups (Figure 8C,D) [38]. RT-qPCR also confirmed that codelivery of H_2S and NO promoted the polarization of macrophages toward an antiinflammatory and proreparative phenotype (Figure 8E).

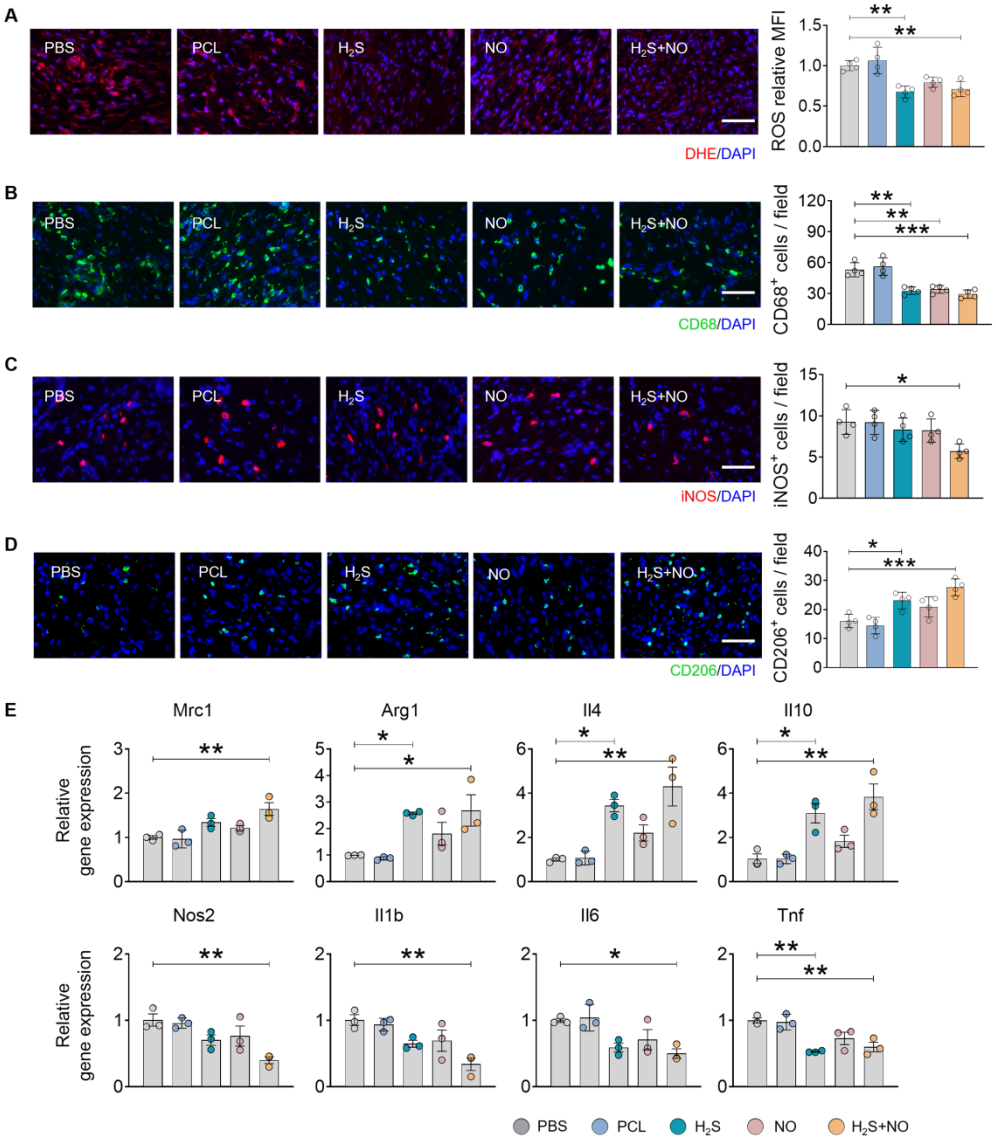

Figure 8. H_2S and NO cooperatively inhibits oxidative stress and modulates inflammation in wound areas. (**A**) DHE staining was performed to detect ROS levels with the quantification of relative MFI (n = 4). Scale bar, 50 μm. (**B**) Immunofluorescence staining for CD68 with the quantification of $CD68^+$ arterioles in wound areas (n = 4). Scale bar,

50 μm. (**C**) Immunofluorescence staining for iNOS with the quantification of $iNOS^+$ cells in wound areas (n = 4). Scale bar, 50 μm. (**D**) Immunofluorescence staining for CD206 with the quantification of $CD206^+$ cells in wound areas (n = 4). Scale bar, 50 μm. (**E**) The relative expression of anti-inflammatory- and proinflammatory- related genes by RT–qPCR (n = 3). Statistical significance was assessed by One-way ANOVA with Tukey's post-hoc analysis. Data are presented as the means ± SEM. * $p < 0.05$, ** $p < 0.01$ and *** $p < 0.001$.

4. Conclusions

In summary, we developed a hybrid prodrug (TSNO) for the codelivery of H_2S and NO that is controlled by GSH and the engineered enzyme A4-β-Gal^{H363A}. TSNO was further incorporated into an electrospun PCL mat for the fabrication of a functional wound dressing. The therapeutic efficacy of the functional dressing was systematically evaluated in a mouse model of full-thickness cutaneous wound. The results demonstrated that controlled release of H_2S and NO cooperatively accelerated wound healing compared to the group treated with H_2S or NO alone. Codelivery of H_2S and NO synergistically promotes collagen deposition, enhances angiogenesis, and modulates inflammation, all of which lead to enhanced tissue regeneration and remodeling.

Our study also has several limitations. First, although the codelivery of H_2S and NO form TSNO has been confirmed in vitro, measuring the H_2S and NO release profile from the patch in vivo remains challenging. Second, the synergistic mechanism by which H_2S and NO promote tissue regeneration and remodeling requires further investigation. Third, only a wound model in healthy mice was established; large animal models are needed in the future to further reveal the translational potential of this functional wound dressing.

Supplementary Materials

The additional data and information can be downloaded at: https://media.sciltp.com/articles/others/2509191607584515/RMD-2508000059-Supplementary-materials-R1.pdf. Figure S1: NMR spectrum of compound 1; Figure S2: NMR spectrum of compound 2; Figure S3: NMR spectrum of compound 3; Figure S4: NMR spectrum of compound 5; Figure S5: NMR spectrum of compound 6; Figure S6: NMR spectrum of compound 7; Figure S7: NMR spectrum of compound SNO; Figure S8: NMR spectrum of compound 8; Figure S9: NMR and HRMS spectrum of compound TSNO; Figure S10: In vitro release of H_2S and NO from the TSNO prodrug; Figure S11: The characterization of TSNO-functionalized wound dressing; Figure S12: HNO production from the interaction of H_2S and NO; Table S1: Primer sequences of qPCR.

Author Contributions

M.Q.: Conceptualization, Investigation, Methodology, Data analysis, Validation, Writing-original draft; G.J.: Investigation, Methodology, Data analysis, Validation, Writing-original draft; P.L.: Methodology, Data analysis; Y.Z.: Investigation, Methodology, Data analysis; W.D.: Methodology, Data analysis; Z.X.: Methodology, Data analysis; H.W.: Data analysis; J.C.: Conceptualization, Supervision, Q.Z.: Conceptualization, Supervision, Project administration, Writing-review & editing, Funding acquisition. All authors have read and agreed to the published version of the manuscript.

Funding

This study is supported by National Natural Science Foundation of China (Nos: 82330066 and 823B2048) and Natural Science Foundation of Tianjin of China (24JCYBJC02000).

Institutional Review Board Statement

All experiments and animal procedures were approved by the Animal Experiments Ethical Committee of Nankai University (2025-SYDWLL-000516).

Informed Consent Statement

Not applicable.

Data Availability Statement

The data in the current study is available from the corresponding author on reasonable request.

Conflicts of Interest

The authors declare that they have no competing financial interests.

References

1. Peña, O.A.; Martin, P. Cellular and molecular mechanisms of skin wound healing. *Nat. Rev. Mol. Cell Biol.* **2024**, *25*, 599–616.
2. Veith, A.P.; Henderson, K.; Spencer, A.; et al. Therapeutic strategies for enhancing angiogenesis in wound healing. *Adv. Drug Deliv. Rev.* **2019**, *146*, 97–125.
3. Zhang, Q.; Gu, R.; Dai, Y.; et al. Molecular mechanisms of ubiquitination in wound healing. *Biochem. Pharmacol.* **2025**, *231*, 116670.
4. Lundberg, J.O.; Weitzberg, E. Nitric oxide signaling in health and disease. *Cell* **2022**, *185*, 2853–2878.
5. Kolluru, G.K.; Shackelford, R.E.; Shen, X.; et al. Sulfide regulation of cardiovascular function in health and disease. *Nat. Rev. Cardiol.* **2023**, *20*, 109–125.
6. Zhu, D.; Hou, J.; Qian, M.; et al. Nitrate-functionalized patch confers cardioprotection and improves heart repair after myocardial infarction via local nitric oxide delivery. *Nat. Commun.* **2021**, *12*, 4501.
7. Pinto, R.V.; Carvalho, S.; Antunes, F.; et al. Emerging nitric oxide and hydrogen sulfide releasing carriers for skin wound healing therapy. *ChemMedChem* **2022**, *17*, e202100429.
8. Malone-Povolny, M.J.; Maloney, S.E.; Schoenfisch, M.H. Nitric oxide therapy for diabetic wound healing. *Adv. Healthc. Mater.* **2019**, *8*, e1801210.
9. Zhou, X.; Wang, H.; Zhang, J.; et al. Functional poly(ε-caprolactone)/chitosan dressings with nitric oxide-releasing property improve wound healing. *Acta Biomater.* **2017**, *54*, 128–137.
10. Zhang, Y.X.; Jing, M.R.; Cai, C.B.; et al. Role of hydrogen sulphide in physiological and pathological angiogenesis. *Cell Prolif.* **2023**, *56*, e13374.
11. Rong, F.; Bao, W.; Li, G.; et al. Aminopeptidase N-activated self-immolative hydrogen sulfide donor for inflammatory response-specific wound healing. *Angew. Chem. Int. Ed. Engl.* **2025**, *64*, e202423527.
12. Zhao, S.; Zhao, W.; Wang, N.; et al. A sustained H_2S-releasing nanocellulose-based hydrogel with anti-inflammatory and antibacterial properties for promoting infected wound healing. *Carbohydr. Polym.* **2025**, *355*, 123424.
13. Cirino, G.; Szabo, C.; Papapetropoulos, A. Physiological roles of hydrogen sulfide in mammalian cells, tissues, and organs. *Physiol. Rev.* **2023**, *103*, 31–276.
14. Ye, S.; Jin, N.; Liu, N.; et al. Gases and gas-releasing materials for the treatment of chronic diabetic wounds. *Biomater. Sci.* **2024**, *12*, 3273–3292.
15. Yuan, S.; Patel, R.P.; Kevil, C.G. Working with nitric oxide and hydrogen sulfide in biological systems. *Am. J. Physiol. Lung Cell. Mol. Physiol.* **2015**, *308*, L403–L415.
16. Ivanovic-Burmazovic, I.; Filipovic, M.R. Saying NO to H_2S: A story of HNO, HSNO, and SSNO. *Inorg. Chem.* **2019**, *58*, 4039–4051.
17. Liu, Q.; Ji, G.; Chu, Y.; et al. Enzyme-responsive hybrid prodrug of nitric oxide and hydrogen sulfide for heart failure therapy. *Chem. Commun.* **2022**, *58*, 7396–7399.
18. Wu, D.; Hu, Q.; Xiong, Y.; et al. Novel H_2S-NO hybrid molecule (ZYZ-803) promoted synergistic effects against heart failure. *Redox Biol.* **2018**, *15*, 243–252.
19. Deng, W.; Xu, Z.; Hua, T.; et al. Targeted codelivery of nitric oxide and hydrogen sulfide for enhanced antithrombosis efficacy. *Bioact. Mater.* **2025**, *48*, 29–42.
20. Lee, M.; McGeer, E.; Kodela, R.; et al. NOSH-aspirin (NBS-1120), a novel nitric oxide and hydrogen sulfide releasing hybrid, attenuates neuroinflammation induced by microglial and astrocytic activation: A new candidate for treatment of neurodegenerative disorders. *Glia* **2013**, *61*, 1724–1734.
21. Li, N.; Huang, C.; Zhang, J.; et al. Chemotactic NO/H_2S nanomotors realizing cardiac targeting of G-CSF against myocardial ischemia-reperfusion injury. *ACS Nano* **2023**, *17*, 12573–12593.
22. Fu, J.; Mao, Y.; Han, J.; et al. A nitric oxide and hydrogen sulfide dual-donating nanosystem for highly synergistic gas-radiotherapy against hepatocellular carcinoma. *Biomater. Adv.* **2023**, *144*, 213209.
23. Xu, S.; Shieh, M.; Paul, B.D.; et al. Hydrogen sulfide: Recent development of its dual donors and hybrid drugs. *Br. J. Pharmacol.* **2023**, *8*, 1–13.
24. Hao, T.; Ji, G.; Qian, M.; et al. Intracellular delivery of nitric oxide enhances the therapeutic efficacy of mesenchymal stem cells for myocardial infarction. *Sci. Adv.* **2023**, *9*, eadi9967.
25. Hou, J.; Pan, Y.; Zhu, D.; et al. Targeted delivery of nitric oxide via a 'bump-and-hole'-based enzyme-prodrug pair. *Nat. Chem. Biol.* **2019**, *15*, 151–160.
26. Yang, S.; Jiang, H.; Qian, M.; et al. MSC-derived sEV-loaded hyaluronan hydrogel promotes scarless skin healing by immunomodulation in a large skin wound model. *Biomed. Mater.* **2022**, *17*, 034104.
27. Zhao, Y.; Biggs, T.D.; Xian, M. Hydrogen sulfide (H_2S) releasing agents: Chemistry and biological applications. *Chem. Commun.* **2014**, *50*, 11788–11805.

28. Huang, H.; Qian, M.; Liu, Y.; et al. Genetically engineered mesenchymal stem cells as a nitric oxide reservoir for acute kidney injury therapy. *eLife* **2023**, *12*, e84820.
29. Moraes, L.A.; Pimpim, R.S.; Eberlin, M.N. Novel Ketalization reaction of acylium ions with diols and analogues in the gas phase. *J. Org. Chem.* **1996**, *61*, 8726–8727.
30. Rodrigues, M.; Kosaric, N.; Bonham, C.A.; et al. Wound healing: A cellular perspective. *Physiol. Rev.* **2019**, *99*, 665–706.
31. Xiong, M.; Yang, X.; Shi, Z.; et al. Programmable artificial skins accomplish antiscar healing with multiple appendage regeneration. *Adv. Mater.* **2024**, *36*, e2407322.
32. Shi, Z.; Yao, C.; Shui, Y.; et al. Research progress on the mechanism of angiogenesis in wound repair and regeneration. *Front. Physiol.* **2023**, *14*, 1284981.
33. Hao, T.; Qian, M.; Zhang, Y.; et al. An injectable dual-function hydrogel protects against myocardial ischemia/reperfusion injury by modulating ROS/NO disequilibrium. *Adv. Sci.* **2022**, *9*, e2105408.
34. Kolluru, G.K.; Shen, X.; Kevil, C.G. A tale of two gases: NO and H_2S, foes or friends for life? *Redox Biol.* **2013**, *1*, 313–318.
35. Eberhardt, M.; Dux, M.; Namer, B.; et al. H_2S and NO cooperatively regulate vascular tone by activating a neuroendocrine HNO-TRPA1-CGRP signalling pathway. *Nat. Commun.* **2014**, *5*, 4381.
36. Lu, Y.Z.; Nayer, B.; Singh, S.K.; et al. CGRP sensory neurons promote tissue healing via neutrophils and macrophages. *Nature* **2024**, *628*, 604–611.
37. Hassanshahi, A.; Moradzad, M.; Ghalamkari, S.; et al. Macrophage-Mediated Inflammation in Skin Wound Healing. *Cells* **2022**, *11*, 2953.
38. Chen, S.; Saeed, A.; Liu, Q.; et al. Macrophages in immunoregulation and therapeutics. *Signal Transduct. Target Ther.* **2023**, *8*, 207.